1996-06

Local area navigation using sonar feature extraction and model based predictive control

Marco, D.B.

Local Area Navigation Using Sonar Feature Extraction And Model Based Predictive Control

D. B. Marco and A. J. Healey
Autonomous Underwater Vehicles Laboratory, Dept. of Mechanical Engineering
Naval Postgraduate School, Monterey, CA. 93943

Abstract

This paper demonstrates a method to navigate an autonomous underwater vehicle in a local area using an acoustic sensor for position information derived from feature detection. A dynamic model of the vehicle response is used for control between location updates. Favorable results have been found using this approach, and precision positioning of the vehicle to centimeters has been accomplished.

Another part of the problem is the need to provide a high frequency update of vehicle position in order to close the positioning servo loops. Using sonar image feature extraction is necessarily time consuming and therefore is performed in a Tactical level process providing asynchronous data to the Tactical navigator. It follows that some form of fast dead reckoning must be performed in the Execution level either by INS/Doppler or by water speed and heading data or by a model based predictor. This paper deals with the use of a model based predictor technique where knowledge of the dynamic model of the vehicle provides state information to the vehicle positioning control function. The model uncertainty provides errors of course, but these are corrected through asynchronous updates from the feature extracted positions in the Tactical level sonar manager. This concept has been verified by both simulation studies and by experimental validation with the NPS Phoenix vehicle.

1. Introduction

While there has always been a need to determine the global position of an underwater vehicle, in some missions involving search, mapping, and intervention with objects, navigation to local area landmarks is more appropriate and precise. All aspects of autonomous search have been of interest to us for some time now, and we have recently developed and extended our robot control system architecture using Prolog as a rule based mission specification language to drive vehicle missions involving motion around targets of interest. In particular, we have studied the use of onboard scanning sonar to perform local area navigation.

In this paper, we attempt to give an elaborate analysis of local area maneuvering using sonar based feature detection from the local scene. A mathematical model of the vehicle response is used to provide control inputs during periods when sonar updates are not available and the experimental results indicate that this method will supplement other techniques where positioning precision to centimeters is necessary.

2. Background

Recent developments in underwater robotics are aimed at providing solutions to the problems of commercial, scientific, and military missions in the coastal ocean environment. Small autonomous vehicles will be able to monitor, search and survey areas of the ocean floor in shallow water. Providing results in near to real time, supervised autonomous activity including mission replanning and system reconfiguration can be used to inspect and monitor underwater structures, harbor environments, and obtain minefield reconnaissance data.

Two classes of mission arise. The survey mission requires an energy efficient vehicle to cruise and follow designated way points whilst taking relevant oceanographic data. The second (the intervention mission) requires a vehicle capable of slow speed and even station keeping with thrusters and servo control to objects using vision, sonar, tactile sensors, or combinations thereof. Examples of survey vehicles include the Odyssey [1], and the Ocean Voyager [2], Remus [3] and the larger vehicles such as the Draper UUV [4] and the Navy's LDUUV [5], while examples of thruster controlled vehicles include the OTTER [6], the Phoenix [7], the Marius [8] and Vortex [9], and the entire class of Remotely Operated Vehicles called ROV's [10].

In the class of vehicles designed for the intervention mission, Marks, et. al. [6] have studied the problem of servo positioning the OTTER vehicle to visual cues from stereoscopic cameras although monocular video data was used to perform edge detection and servo control of the pan and tilt mounting coupled to the vehicle platform. Some of the co-authors of this paper have reported positioning control of the Phoenix vehicle to acoustic returns from high frequency (1.2Mhz.) sonar where the sonar was integrated into the execution level control software [11] as necessary to the stabilization of the vehicle motion. Part of the problem lies in the need

0-7803-3185-0/96$5.00©1996 IEEE

for improved modeling of thruster behavior as described in Yoerger [12], and Healey et. al. [13]. Once maneuvering control around objects in the local area scene is understood to a satisfactory degree, intervention using manipulators and other tactile devices will be enabled. Such activities as changing out a battery pack for a bottom mounted sensor or finding and entering an underwater garage for repowering will then become commonplace.

We focus first on the problem of local area navigation and maneuvering using model based control and acoustic feature extraction techniques for precise positioning.

3. Model Based Control Formulation

Absent of an inertial position reference, where sonar position updates are asynchronous, and occur at times much longer than the control frequency of 10 Hz, a dynamic model of the vehicle is used for state information between updates. A three degree-of-freedom model (longitudinal, lateral, and heading) is used since the motion is restricted to the horizontal plane with the depth maintained by a separate controller. The model including drag, added mass, and steady state thrust for surge is

$$M_x\dot{u}(t) + b_x u(t)|u(t)| = 2\alpha_x \mathrm{v}_x(t)|\mathrm{v}_x(t)| \qquad (1)$$

The sway directional equation of motion is

$$\begin{aligned} \mathrm{M}_y\,\dot{v}(t) + b_y v(t)|v(t)| = \\ \alpha_y \mathrm{v}_{blt}(t)|\mathrm{v}_{blt}(t)| + \alpha_y \mathrm{v}_{slt}(t)|\mathrm{v}_{slt}(t)| \end{aligned} \qquad (2)$$

and finally the yaw equation of motion becomes

$$\begin{aligned} I_z\,\dot{r}(t) + b_\psi r(t)|r(t)| = \\ \alpha_\psi\, \mathrm{v}_{blt}(t)|\mathrm{v}_{blt}(t)| - \alpha_\psi\, \mathrm{v}_{slt}(t)|\mathrm{v}_{slt}(t)| \end{aligned} \qquad (3)$$

where

$$\begin{aligned} M_x &= m + m_{ax}, \\ M_y &= m + m_{ay}, \\ I_z &= I_{zz} + I_{azz} \end{aligned}$$

and

$$\mathrm{v}_x(t)|\mathrm{v}_x(t)| = (\mathrm{v}_{ls}(t)|\mathrm{v}_{ls}(t)| + \mathrm{v}_{rs}(t)|\mathrm{v}_{rs}(t)|)/2$$

m is the vehicle mass, I_{zz} the mass moment of inertia about the body-fixed z-axis, and the subscript "a" refers to the added mass or inertia of the body. $u(t)$, $v(t)$, and $r(t)$ are the body-fixed rates for longitudinal (x-axis), lateral (y-axis), and heading (ψ) directions. b_x, b_y, b_ψ are the square-law damping coefficients, $\mathrm{v}_{ls}(t)$, $\mathrm{v}_{rs}(t)$, and $\mathrm{v}_{blt}(t)$, $\mathrm{v}_{slt}(t)$ are the thruster motor input voltages for the left/right rear screws, and the bow/stern lateral thrusters respectively. The voltage to force/moment coefficients are given by α_x, α_y, and α_ψ.

The above dynamics equations can be formulated using matrix notation as

$$\boldsymbol{M}\dot{\boldsymbol{x}}(t) = \boldsymbol{f}(\boldsymbol{x}(t),\boldsymbol{b}) + \boldsymbol{g}(\alpha)\boldsymbol{u}(t) \qquad (4)$$

and vehicle kinematics are defined by

$$\dot{\boldsymbol{z}}(t) = \boldsymbol{h}(\psi)\boldsymbol{x}(t) + \boldsymbol{u}_c(t). \qquad (5)$$

The body-fixed rates are

$$\boldsymbol{x}(t) = \{\, u(t)\ \ v(t)\ \ r(t)\,\}^T,$$

the global position and orientation is given by

$$\boldsymbol{z}(t) = \{\, X(t)\ \ Y(t)\ \ \psi(t)\,\}^T.$$

The vector describing the hydrodynamic drag that is a function of the body-fixed rates and square-law damping coefficients, $\boldsymbol{b} = \{\, b_x\ \ b_y\ \ b_\psi\,\}$ is

$$\boldsymbol{f}(\boldsymbol{x}(t),\boldsymbol{b}) = \begin{Bmatrix} -b_x u(t)|u(t)| \\ -b_y v(t)|v(t)| \\ -b_\psi r(t)|r(t)| \end{Bmatrix},$$

the mass matrix is

$$\boldsymbol{M} = \begin{bmatrix} M_x & 0 & 0 \\ 0 & M_y & 0 \\ 0 & 0 & I_z \end{bmatrix},$$

and input gain matrix which is solely a function of the thruster coefficients, $\alpha = \{\, \alpha_x\ \ \alpha_y\ \ \alpha_\psi\,\}$ is

$$\boldsymbol{g}(\alpha) = \begin{bmatrix} 2\alpha_x & 0 & 0 \\ 0 & \alpha_y & \alpha_y \\ 0 & \alpha_\psi & -\alpha_\psi \end{bmatrix}$$

Finally, the control input vector is defined as

$$\boldsymbol{u}(t) = \begin{Bmatrix} \mathrm{v}_x(t)|\mathrm{v}_x(t)| \\ \mathrm{v}_{blt}(t)|\mathrm{v}_{blt}(t)| \\ \mathrm{v}_{slt}(t)|\mathrm{v}_{slt}(t)| \end{Bmatrix}. \qquad (6)$$

For the case of translation in X, Y and rotation ψ, the transformation matrix from the body-fixed axes to the global reference is given by

$$\boldsymbol{h}(\psi(t)) = \begin{bmatrix} cos(\psi(t)) & -sin(\psi(t)) & 0 \\ sin(\psi(t)) & cos(\psi(t)) & 0 \\ 0 & 0 & 1 \end{bmatrix}, \quad (7)$$

and it's time derivative is

$$\dot{\boldsymbol{h}}(\psi(t), \dot{\psi}(t)) = \begin{bmatrix} -\dot{\psi}(t)sin(\psi(t)) & -\dot{\psi}(t)cos(\psi(t)) & 0 \\ \dot{\psi}(t)cos(\psi(t)) & -\dot{\psi}(t)sin(\psi(t)) & 0 \\ 0 & 0 & 0 \end{bmatrix}$$

Any current disturbances are represented by

$$\boldsymbol{u}_c(t) = \{ u_c(t) \;\; v_c(t) \;\; r_c(t) \}^T$$

where the elements of $\boldsymbol{u}_c(t)$ are the body-fixed current rates.

The sliding mode control law can now be formulated defining the tracking error vector in terms of global coordinates as

$$\begin{bmatrix} \dot{\tilde{z}}(t) \\ \tilde{z}(t) \end{bmatrix} = \begin{bmatrix} \dot{z}_{com}(t) \\ z_{com}(t) \end{bmatrix} - \begin{bmatrix} \dot{z}(t) \\ z(t) \end{bmatrix}. \quad (8)$$

The subscript "*com*" refers to the commanded value of the position or rate in question, where commanded time variations of states must be consistent with vehicle physical capabilities and usually come from separate path planning algorithms.

Since the dynamics equation is in terms of body-fixed rates and accelerations, Equation (8) can be expressed in terms of body-fixed rates using Equation (5). If $\boldsymbol{u}_c(t)$ is assumed zero:

$$\begin{bmatrix} \boldsymbol{h}(\psi(t))\tilde{\boldsymbol{x}}(t) \\ \tilde{z}(t) \end{bmatrix} = \begin{bmatrix} \boldsymbol{h}(\psi(t))\boldsymbol{x}_{com}(t) \\ z_{com}(t) \end{bmatrix} - \begin{bmatrix} \boldsymbol{h}(\psi(t))\boldsymbol{x}(t) \\ z(t) \end{bmatrix}. \quad (9)$$

Now that the tracking error has been formulated, an equation defining the sliding surface in terms of this error can be written as

$$\sigma(\tilde{\boldsymbol{x}}(t), \tilde{z}(t)) = \begin{bmatrix} \boldsymbol{S}_1 & \boldsymbol{S}_2 \end{bmatrix} \begin{bmatrix} \boldsymbol{h}(\psi(t))\tilde{\boldsymbol{x}}(t) \\ \tilde{z}(t) \end{bmatrix} \quad (10)$$

where

$$\sigma(\tilde{\boldsymbol{x}}(t), \tilde{z}(t)) \in \Re^{3\times 1}; \quad \boldsymbol{S}_1, \boldsymbol{S}_2 \in \Re^{3\times 3}$$

The elements of $\boldsymbol{S}_1$ and $\boldsymbol{S}_2$ can be selected to provide the desired performance of the closed loop system. For the case of planar control, these become

$$\boldsymbol{S}_1 = \begin{bmatrix} 1 & 0 & 0 \\ 0 & 1 & 0 \\ 0 & 0 & 1 \end{bmatrix} \quad \boldsymbol{S}_2 = \begin{bmatrix} \lambda_x & 0 & 0 \\ 0 & \lambda_y & 0 \\ 0 & 0 & \lambda_\psi \end{bmatrix}$$

To ensure that stable tracking behavior is achieved, the condition:

$$\lim_{t\to\infty} \dot{\sigma}(\tilde{\boldsymbol{x}}(t), \tilde{z}(t)) \to 0$$

with

$$\lim_{t\to\infty} \sigma(\tilde{\boldsymbol{x}}(t), \tilde{z}(t)) \to 0$$

will also imply

$$\tilde{\boldsymbol{x}}(t), \tilde{z}(t) \to 0 \text{ as } t \to \infty.$$

The condition that $\sigma(\tilde{\boldsymbol{x}}(t), \tilde{z}(t))$ is always decreasing can be established if a Lyapunov function of the sliding surface is formed as

$$V(t) = \frac{1}{2}\sigma^T(\tilde{\boldsymbol{x}}(t), \tilde{z}(t)) * \sigma(\tilde{\boldsymbol{x}}(t), \tilde{z}(t)), \quad (11)$$

and

$$\dot{V}(t) = \dot{\sigma}^T(\tilde{\boldsymbol{x}}(t), \tilde{z}(t)) * \dot{\sigma}(\tilde{\boldsymbol{x}}(t), \tilde{z}(t)) \quad (12)$$

Global asymptotic stability is guaranteed if $V(t)$ is positive definite and $\dot{V}(t)$ is negative definite. The quadratic nature of (11) assures the positive definiteness of $V(t)$, while negative definiteness of $\dot{V}(t)$ requires that

$$\dot{\sigma}_i(\tilde{\boldsymbol{x}}(t), \tilde{z}(t)) = -\eta_i sgn(\sigma_i(\tilde{\boldsymbol{x}}(t), \tilde{z}(t))) \quad i = x, y, \psi \quad (13)$$

where each η_i is a positive scalar matched with each control direction, x, y, and ψ. The positive definiteness of $V(t)$ and the negative definiteness of $\dot{V}(t)$, implies that given any initial condition, $\sigma(\tilde{\boldsymbol{x}}(0), \tilde{z}(0))$, $\sigma(\tilde{\boldsymbol{x}}(t), \tilde{z}(t))$ will remain bounded such that

$$V(\sigma(\tilde{x}(t), \tilde{z}(t)) \leq V(\sigma(\tilde{x}(0), \tilde{z}(0)).$$

Since $sgn(\sigma_i(\tilde{x}(t), \tilde{z}(t)))$ is discontinuous across $\sigma(\tilde{x}(t), \tilde{z}(t)) = 0$, undesirable switch chattering can occur. This is alleviated by the use of a "boundary layer" around zero. Therefore, instead of using a *sgn* function, a continuous form is preferred such that

$$sat(\sigma_i(\tilde{x}(t), \tilde{z}(t))./\phi_i) = \begin{cases} sgn(\sigma_i(\tilde{x}(t), \tilde{z}(t))) & \text{if } |\sigma_i(\tilde{x}(t), \tilde{z}(t))| > \phi_i \\ \sigma_i(\tilde{x}(t), \tilde{z}(t)) / \phi_i & \text{otherwise} \end{cases}$$

where "./" denotes element by element division. Another approach is to simply use the continuous function $tanh(\sigma(\tilde{x}(t), \tilde{z}(t)))$. Substituting the definition of *sat* into Equation (13) and noting Equation (10), it can be written in a more compact form as

$$\dot{\sigma}(\tilde{x}(t), \tilde{z}(t)) = S_1\dot{h}(\psi(t))\tilde{x}(t) + S_1 h(\psi(t))\dot{\tilde{x}}(t) + S_2\dot{\tilde{z}}(t) = -F(\sigma(\tilde{x}(t), \tilde{z}(t)), \phi) \quad (14)$$

Substituting the dynamics equation (1) into (14) yields the control solution, $u(t)$, and since the matrices $f(\bullet)$, $g(\bullet)$, and $h(\bullet)$ are uncertain in general, they must be formulated using estimates, denoted as $\hat{f}(\bullet)$, $\hat{g}(\bullet)$, and $\hat{h}(\bullet)$, where the $(\bullet)$ is used for notational compactness. The control vector can be split into three parts

$$u(t) = u_1(t) + u_2(t) + u_3(t)$$

where

$$u_1(t) = \hat{g}(\bullet)^{-1}(\hat{M}\dot{x}_{com}(t) - \hat{f}(\bullet)) \quad (15)$$

contains the acceleration terms,

$$u_2(t) = \hat{g}(\bullet)^{-1}\hat{M}\hat{h}^{-1}(\bullet)(\dot{\hat{h}}(\bullet)\hat{h}(\bullet)^{-1} + S_1^{-1}S_2)\dot{\tilde{z}}(t) \quad (16)$$

contains the velocity terms, and finally

$$u_3(t) = \hat{g}(\bullet)^{-1}\hat{M}\hat{h}^{-1}(\bullet)S_1^{-1}F(\sigma(\bullet), \phi) \quad (17)$$

is the switching term, where

$$\dot{x}_{com}(t) = \hat{h}^{-1}(\bullet)(-\dot{\hat{h}}(\bullet)\hat{h}(\bullet)^{-1}\dot{z}_{com}(t) + \ddot{z}_{com}(t))$$

S_1 is identity, and if all commanded velocities and accelerations are zero the control reduces to

$$u_1(t) = \hat{g}(\bullet)^{-1}\hat{f}(\bullet)$$
$$u_2(t) = -\hat{g}(\bullet)^{-1}\hat{M}\hat{h}^T(\bullet)[\dot{\hat{h}}(\bullet)\hat{h}^T(\bullet) + S_2)\dot{\hat{z}}(t)$$
$$u_3(t) = \hat{g}(\bullet)^{-1}\hat{M}\hat{h}^T(\bullet)F(\hat{\sigma}(\bullet), \phi) \quad (18)$$

where $u_1(t)$, $u_2(t)$, and $u_3(t)$ contain the acceleration, velocity and switching terms respectively.

4. Target Detection with Sonar

To perform local area navigation using sonar, it is necessary to select an easily discernible feature in the vehicle operating area and use it as a fixed reference. The target feature should be stationary and reasonably unique with respect to other structures in the sonar field of view. This will be necessary to enable repeatable and unambiguous detection of the reference feature. In order to classify these features, each must be segmented into a separate object and analyzed to see if it posses the structural properties of the desired target for reference.

For the results presented in this paper, the target used for the local navigation reference was a 0.5 meter diameter, 0.75 meter long cylinder placed vertically in the water column of the NPS AUV test tank which measures 6.0 by 6.0 meters square and 1.8 meters deep. A Tritech ST1000 profiling sonar head was used which is mounted vertically in the nose of the NPS Phoenix vehicle. The head uses a stepper motor which can mechanically rotate the transducer through 360^o with respect to it's mounting at a minimum angular resolution of 0.9^o. For each step, the sonar is pinged and a single range value is returned which enables a complete profile of the area surrounding the vehicle to be constructed.

An actual scan of the cylindrical target and square tank walls is shown in Figure 2. A sweep width of $\pm 35^o$ and angular resolution of 1.8^o was used. Each dot or "pixel" corresponds to a discrete range value returned by the sonar for a given angular position of the transducer head. Several disjoint groups or segments of pixels are visible in the field of view: the two sections of the tank wall, and the cylinder which casts an acoustic shadow against the wall. Since sonar range drop outs and noise are common with sonars, the tank wall to the upper right of the cylinder is broken up into several segments, although in reality, it is a continuous feature. It is this nature of acoustic sensors that lead to the development of the following algorithms for cylinder detection in the NPS test tank.

Since the cylinder is the desired target for the local area reference, returns from the tank walls need to be filtered out and ignored. This can be accomplished by segmenting each contiguous, disjoint group of range pixels and analyzing them for the desired characteristics of a cylinder. The method to isolate these segments is outlined in the flow diagram in Figure 3. The filter is

initialized by pinging at a fixed bearing to obtain an average range value, $\bar{r}$. Once this is done, the head is commanded to scan in a clockwise direction and each range return is first tested for feasibility. If the range is zero or if it exceeds the maximum operating range, r_{max}, it is ignored and that range, r_i, is set to the current average range, $\bar{r}$, and the scan proceeds. If the range is feasible, a test is performed to see if it lies within an error band of $\pm \Delta r$ of the average and if so, the value of $\bar{r}$ is recalculated using the new range. The range and the associated bearing angle is then stored in a vector of size n, the number of pixels defining the segment. If the range falls outside of the error band, a flag is set to examine how closely subsequent returns compare to the new range. A secondary average, $\bar{r}_{new}$, is initialized to this value and a new segment is declared if the next n_{min} adjacent ranges are consistent with this average at which time the current average is set to $\bar{r}_{new}$. The old segment is now terminated at $i - n_{min}$ and the range, bearing and pixel count values are processed to extract any shape information they may provide. If the subsequent ranges, less than n_{min} pixels are inconsistent with $\bar{r}_{new}$, and fall near the previous average, a new segment is not assumed and the scan continues using $\bar{r}$. These "false alarms" occur quite frequently due to the nature of the sonar returns which contain drop outs and false ranges. The value of n_{min} can be varied depending on the environment of operation. For the test tank which provides relatively clean signals, the value of n_{min} is typically 3, but in more noisy conditions, a larger value should be used to provide higher filtering.

Once a separate segment has been identified, the vector containing it's ranges and bearing angles is analyzed. The flow diagram for this algorithm is shown in Figure 4. To determine if the object defined by the segment is a cylinder, it must posses the following characteristics:

1. Consist of a sufficient number of pixels, n, that does not exceed a maximum, n_{max}. If the number of pixels is large, in this case greater than 10 it can be safely assumed the segment is a wall due the relative size of the cylinder.
2. Be in front of the tank walls. This is an obvious observation since the cylinder is assumed to be in the tank but must be included in the algorithm to avoid confusion by perceived cylindrical shaped areas on the wall due to noise.
3. Have a central range closer than it's edges. Since a cylinder appears the same from any direction in a horizontal plane, the center of the segment will always be closer the sonar than the beginning and ending edges.

The preceding algorithms have been used with much success in the NPS test tank and should operate well in an open water environment especially since the tank walls will be absent and the reference target the most visible object in the area. This procedure can be modified to search for other geometric shapes since the idea of segmentation of each feature is retained but does not attempt to supplant more sophisticated and robust pattern recognition algorithms available. This method was adopted since it can be executed in real time and is simply used as a means to perform the tasks described in the following sections.

5. Relative Position Estimation

Once the reference target has been identified, it becomes the origin of the navigation coordinate frame where the X-axis is aligned with heading 0 degrees and the Y-axis along a heading of 90^{o} as shown in Figure 5. The two dimensional position vector to the origin of the vehicle body-fixed reference with respect to the navigation frame at detection time T is

$$\boldsymbol{R}_v(T) = \begin{Bmatrix} X_v(T) \\ Y_v(T) \end{Bmatrix} = -(\boldsymbol{r}_s(T) + \boldsymbol{R}_{cyl}(T)) \tag{19}$$

where

$$\boldsymbol{r}_s(T) = \boldsymbol{h}(\psi(T)) \begin{Bmatrix} x_s \\ y_s \end{Bmatrix},$$

and x_s, y_s is the position of the sonar head in vehicle coordinates.

$$\boldsymbol{R}_{cyl}(T) = \begin{Bmatrix} (R_{cyl}(T) + r_{cyl})\cos(\psi(T) + \psi_s(T)) \\ (R_{cyl}(T) + r_{cyl})\sin(\psi(T) + \psi_s(T)) \end{Bmatrix} \tag{20}$$

where $R_{cyl}(T)$ is the sonar range to the target, $\psi_s(T)$ is the heading angle of the sonar beam, and for the case of a cylindrical target, r_{cyl} is it's radius. After the target has been found, and the location of the vehicle is determined, the sonar is commanded to sweep across it at a prescribed angular sweep width denoted ψ_{sw} about a heading which is the center of the target. This reduces the amount of delay time between re-acquiring the target.

6. Position Update

Since there is a delay time of up to 10 seconds between target detections, the vehicle control must use a dynamic model between position updates. Equation (4) is integrated to obtain estimates of the vehicle position denoted $\hat{X}(t)$, and $\hat{Y}(t)$ during this time. The scan

direction command angle $\psi_{sd}(t)$ between position updates is computed using

$$\psi_{sd}(t) = atan2\left(\frac{-(\hat{Y}(t) + x_s sin(\psi(t)) + y_s cos(\psi(t)))}{-(\hat{X}(t) + x_s cos(\psi(t)) + y_s sin(\psi(t)))}\right) - \psi(t) \quad (21)$$

and a maneuver using this approach is shown in Figure 6. If the target has not been reaquired within a specified time, the head is commanded to return to continuous sweep mode. This is needed if the scan width is too narrow and there exists a large discrepancy between the model and the actual vehicle, since the scan direction calculated from the estimates of position can be in error. One approach to reduce this possibility is to increase the scan width, ψ_{sw} to say 120^0 degrees but doing this will increase the time between updates and has not been done for this series of experiments.

For vehicle control in a plane, the complete state is defined by

$$\boldsymbol{X}(t) = \{ u(t)\ v(t)\ r(t)\ X(t)\ Y(t)\ \psi(t) \}^T$$

and the block diagram representation of the control scheme is shown in Figure 7. When the cylinder has been identified, the model is asynchronously updated at time of target detection using a Kalman filter of the form

$$\hat{X}(T) = (1 - K)\hat{X}^-(t) + KX_v(T)$$
$$\hat{Y}(T) = (1 - K)\hat{Y}^-(t) + KY_v(T) \quad (22)$$

where

$$K = \frac{\sigma_m^2}{\sigma_m^2 + \sigma_s^2} \quad (23)$$

and σ_m^2 is the variance of the system model estimate of position and σ_s^2 is the variance of vehicle position using the sonar. $\hat{X}^-(t)$, and $\hat{Y}^-(t)$ is the current estimate of position from the model just before the correction from the sonar is obtained. This analysis assumes the position estimate from the sonar is extremely accurate and the model very inaccurate. Therefore, the variance for position from sonar is set to 0 and infinity for the model. This causes the current estimate from the model to be disregard at the time of sonar update and reduces Equation (22) to be simply

$$\hat{X}(T) = X_v(T)$$
$$\hat{Y}(T) = Y_v(T) \quad (24)$$

which states complete confidence in the sonar. At this time the dynamic model of the system is reset to the values obtained from Equation (24) and the model updates from there during the next interval between updates.

The onboard gyroscopes provide the heading angle and yaw rate values at 10 Hz, which are synchronous and highly accurate and no estimation of these is required. The observation vector is defined by

$$y(t) = \boldsymbol{C}\boldsymbol{X}(t) \quad (25)$$

and since only these two measurements made, Equation (25) reduces to

$$y(t) = \begin{Bmatrix} r(t) \\ \psi(t) \end{Bmatrix} \quad (26)$$

which is used each time step in the vehicle controller and dynamic model along with the set point vector

$$\boldsymbol{r}(t) = \begin{Bmatrix} X_{com}(t) \\ Y_{com}(t) \\ \psi_{com}(t) \end{Bmatrix}.$$

7. Experimental Results

A five pose experiment was performed in the NPS hover tank. During execution, all pertinent data was collected, including depth and heading information, all sonar data, and the estimates of position, position rate, and the updates from the sonar. Table 1 shows the commanded position and heading comprising the five poses and are shown in Figure 8.

Table 1. Commanded Mission Poses

Pose	X_{com} (m)	Y_{com} (m)	ψ_{com} (rad)
1	2.13	-2.13	0.0
2	2.13	0.0	0.0
3	2.13	2.13	0.0
4	2.13	0.0	0.5236
5	-2.74	-2.13	0.0

The following tables give the parameter values used in the vehicle model and the sliding mode controller gains.

Table 2. Parameters for Vehicle Model and Sliding Mode Controller Gains

Para-meter	Value	Unit

Gain	Value	Unit

m	194.8	Kg
m_{ax}	19.49	Kg
m_{ay}	155.9	Kg
I_{zz}	53.60	Kg-m^2
I_{zza}	53.60	Kg-m^2
b_x	63.80	Kg/m
b_y	815.4	Kg/m
b_ψ	74.86	Kg-m^2
α_x	0.056	N/V^2
α_y	0.018	N/V^2
α_ψ	0.008	N-m/V^2

λ_x	0.20	rad/s
λ_y	0.20	rad/s
λ_ψ	0.20	rad/s
η_x	0.15	m/s^2
η_y	0.09	m/s^2
η_ψ	0.20	rad/s^2
ϕ_x	0.06	m/s
ϕ_y	0.09	m/s
ϕ_ψ	0.20	rad/s

Note: $\alpha_{slt} = \alpha_{blt} = \alpha_y l_{lt}$, where l_{lt} (0.45 m) is the distance from the mass center of the vehicle to the center of the lateral thruster axes which is the same for both thrusters.

The experiment specified the vehicle to submerge to a depth of 0.4 meters using vertical thrusters as detailed in [14]. Once this depth was reached, the ST1000 sonar was activated and scanned clockwise until the target (cylinder) was identified. At this time, the first pose (1) was issued and the vehicle started the controlled maneuver.

Most control phase transitions of the Phoenix are event based, meaning that a certain set of criteria must be met in order for a transition to occur. A common example of this is when a position set point is sent to the vehicle controllers and reached. A method of determining whether the vehicle has indeed reached this point must be programmed into the control logic. Measuring the position error alone and declaring the maneuver complete when this error is small is not sufficient. This is because the vehicle could be overshooting the commanded position and simply passing through the set point. Therefore, not only must the position error be small but the rate error must also be small. This dual criteria can be expressed mathematically as a positive definite, linear combination of the position error $e(t)$ and the position rate error $\dot{e}(t)$, such that

$$\sigma(t) = \begin{Bmatrix} \sigma_X(t) \\ \sigma_Y(t) \\ \sigma_\psi(t) \end{Bmatrix} = w_e|e(t)| + w_{\dot{e}}|\dot{e}(t)| \qquad (27)$$

where w_e and $w_{\dot{e}}$ are weights for the position and rate errors respectively and for planar motion the errors are

$$e(t) = \begin{Bmatrix} X_{com}(t) - X_v(t) \\ Y_{com}(t) - Y_v(t) \\ \psi_{com}(t) - \psi(t) \end{Bmatrix}$$

and

$$\dot{e}(t) = \begin{Bmatrix} \dot{X}_{com}(t) - \dot{X}(t) \\ \dot{Y}_{com}(t) - \dot{Y}(t) \\ r_{com}(t) - r(t) \end{Bmatrix}$$

This equation allows a minimum value of $\sigma(t)$ for each control direction X, Y, and ψ denoted , σ_{0X}, σ_{0Y}, and $\sigma_{0\psi}$ to be specified defining a threshold for the combination of errors which can be set relatively large when precision control is not required or low for extremely precise positioning. Once each $\sigma(t)$ drops below it's respective σ_0, the maneuver is declared complete and a transition to the next control phase may occur.

For these experiments, the transition was based on position errors from the sonar ranges, not from the model estimates since the model will always predict a very smooth trajectory to the set point. The parameters for the error equation used were $\sigma_{0X} = \sigma_{0Y} = 0.08$ meters, $\sigma_{0\psi} = 0.1$ radians, and $w_e = w_{\dot{e}} = 1.0$.

Figure 9 shows the position response results where the upper trace is $\hat{Y}(t)$ and the lower $\hat{X}(t)$. The position calculated from sonar at update, $X_v(T)$ and $Y_v(T)$ are shown with circles and asterisks respectively. Examining the response for $\hat{X}(t)$ it is evident that the model for the longitudinal direction is in error since the predicted position at the time of correction is about double that calculated with the sonar. This mismatch has been attributed to the absence of shrouds around the rear screws. Without them, an unmodeled transient force lag is present that is common with open propellers. Since this lag was uncompensated, and the control was dictated by the model predictions between position updates, large voltage commands to the screws were of too short a duration to build up sufficient force on the vehicle as shown in Figure 10. The performance was further degraded by the estimated position and rate feedback from the model. As these values were assumed to be nearing the set point pose, the controller actually reversed the propellers (negative voltage command) in an attempt to slow the vehicle. This effect can also be clearly seen in Figure 10 between the time 46.1 seconds and 53.1 seconds, the time of the position update from the sonar. The prediction of the lateral movement, $\hat{Y}(t)$, is much better since the cross-body thrusters are shrouded due to their tunnel design and the model parameters are well established. In all, local dynamic positioning to centimeters is possible in the tank environment.

8. Discussion and Conclusion

The results of these experiments have shown that it is possible to navigate an underwater vehicle in a local area using an acoustic sensor for position information. The accuracy of the model used between updates is moderately satisfactory and can allow for time varying currents. However, some additional model adjustments could be made to compensate for the force lag in the longitudinal direction during transient thrust conditions. This undesirable effect could also be alleviated by the addition of shrouds around the rear screws which should bring the performance up to that of the lateral thrusters. While these results were taken in a tank environment, another improvement would be to fuse the model with an INS system in between updates from the sonar, and then fuse that estimate with the sonar data to obtain a smoother averaging at update time. This would allow for compensation of wave induced disturbances while retaining the positioning precision found. Since the sonars are mechanically scanned, and a delay of up to 10 seconds between position update is common, use of an electronically scanned or multi-beam sonars may be preferable although our experience to date has been that crosstalk between beams can be a serious problem.

Acknowledgment

The authors wish to recognize the financial support of the National Science Foundation under Grant No. BCS-9306252.

References

[1] Bellingham, J. G., Goudey, C. A., et. al. "A Second Generation Survey AUV", Proc. *IEEE Symp. on Autonomous Underwater Vehicle Technology*, July 1994, pp. 148-156.

[2] Smith, S. M., Dunn, S., "The Ocean Voyager II: An AUV Designed for Coastal Oceanography", Procs. *IEEE Symp. on Autonomous Underwater Vehicle Technology*, July 1994, pp. 139-148

[3] Von Alt, C., Allen, B., Austin, T., Stokey, R., "Remote Environmental Measuring Units" *Proceedings of the IEEE Symposium on Autonomous Underwater Vehicle Technology*, AUV '94, July 1994, pp. 13-20.

[4] Brancart, C., "The Evolution of the DARPA / ARPA UUV Program", *Proceedings of the 1994 NSF IARP Workshop on Mobile Robots for Subsea Environments*, MBARI, Pacific Grove, CA. May 1994.

[5] Agoras, C., Lee, C. O., Hills, S., Carlino, D., "U. S. Navy UUV Navigation", *Sea Technology*, January, 1996, pp. 56-60.

[6] Marks, R. L., Rock, S. M., Lee, M. J., "Real Time Video Mosaicking of the Ocean Floor",.*Procs. IEEE Symp. on Auton. Underwater Vehicle Tech.*, July 1994, pp. 21-28.

[7] Healey, A.J., Marco, D. B., "Slow Speed Flight Control of Autonomous Underwater Vehicles: Experimental Results with NPS AUV II" *Proceedings of the 2nd International Offshore and Polar Engineering Conference*, San Francisco, July 14-19 1992.

[8] Pascoal, A., "The AUV MARIUS: Mission Scenarios, Vehicle Design, Construction and Testing", *Proceedings of the 2nd Workshop on Mobile Robotics for Subsea Environments*, Monterey bay Aquarium, Monterey, California, May 1994.

[9] Perrier, M., Rigaud, V., Peuch, A., Coste-Maniere, E., Simon, B., " Vortex: A versatile Testbed Vehicle for Control Algorithms Evaluation", *Proceedings of the 8th. UUST*, Durham New Hampshire, September 27-29, 1993, pp. 29-36.

[10] Newman, J. B., Stakes, D.1994, "Tiburon: Development of an ROV for Ocean Science Research ", *Proc. OCEANS'94*, Brest, France Sept. 1994, Vol. II pp. 483-488.

[11] Healey, A. J., et al., "Coordination of the Hovering Behaviors of the NPS AUV II using Onboard Sonar Servoing", *Proceedings of the 1994 NSF IARP Workshop on Mobile Robots for Subsea Environments*, MBARI, Pacific Grove, CA. May 1994 .

[12] Yoerger, D.R., Cooke, J.G., Slotine, J.J.E., "The Influence of Thruster Dynamics on Underwater Vehicle Behavior and Their Incorporation into Control System Design" *IEEE Journal of Oceanic Engineering*, Vol. 15, No. 3, 1991, pp. 167-178

[13] Healey, A. J., Rock, S. M., Cody, S., Miles, D., Brown, J. P., " Towards an Improved Understanding of Thruster Dynamics for Underwater Vehicles", *IEEE Journal of Oceanic Engineering* Oct. 1995, Vol. 20, No. 4, pp. 354-361.

[14] Healey, A. J., Marco, D. B., McGhee, R.B., "Autonomous Underwater Vehicle Control Coordination Using A Tri-Level Hybrid Software Architecture", *Proceedings of the IEEE Robotics and Automation Conference*, Minneapolis, MI, April 1996.

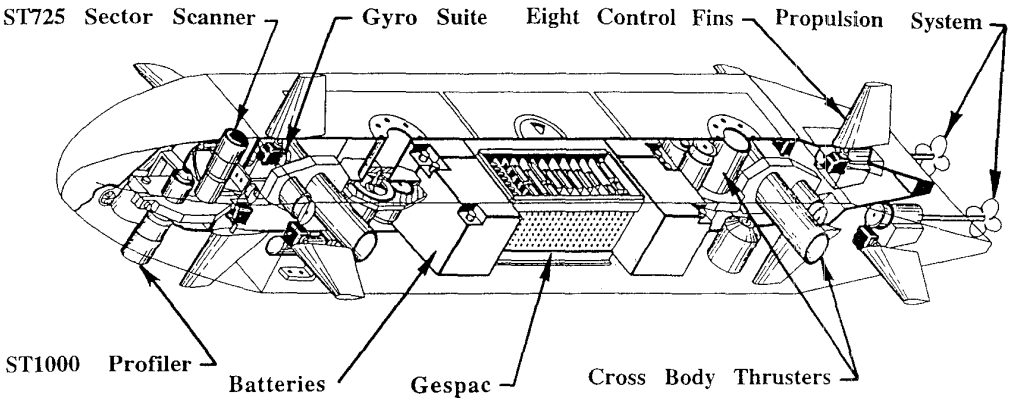

Figure 1. Internal View of the NPS Phoenix

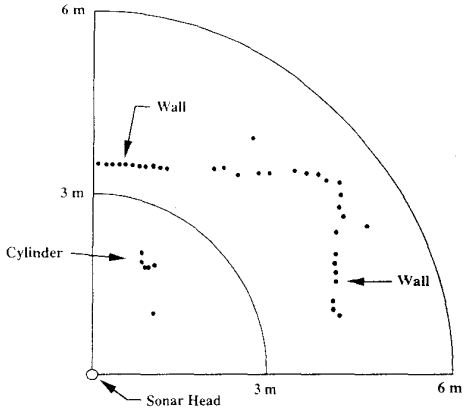

Figure 2. ST1000 Sonar Image of Cylinder and Tank

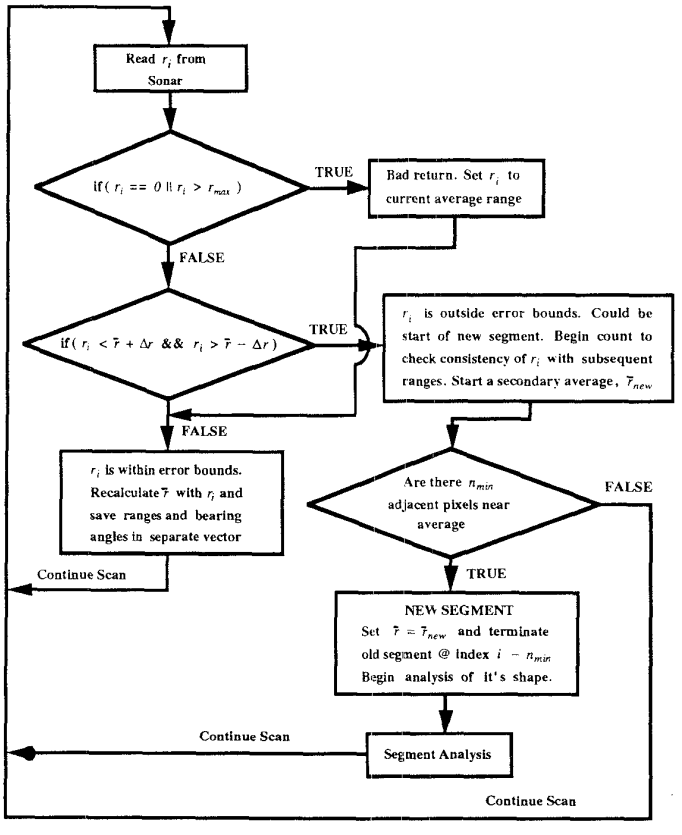

Figure 3. Segmenting Algorithm Flow Diagram

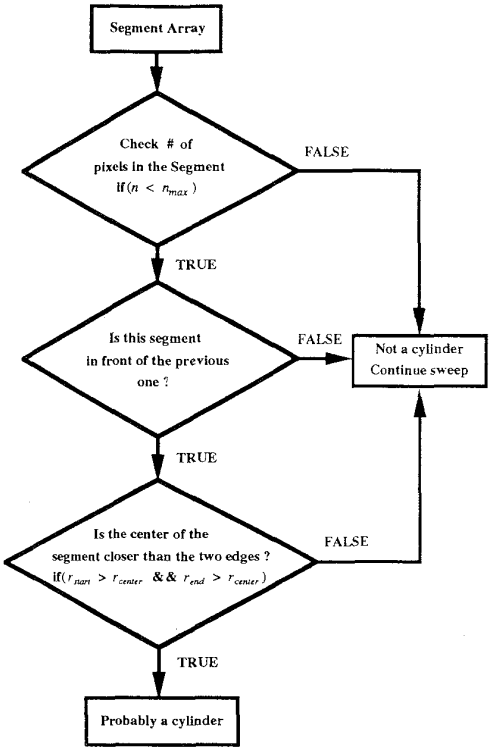

Figure 4. Segment Shape Algorithm Flow Diagram

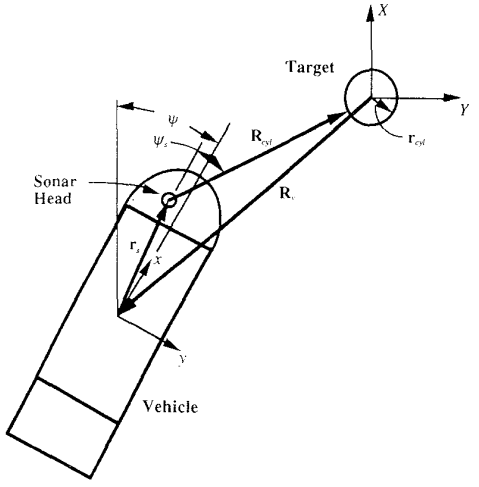

Figure 5. Position Vector Definitions

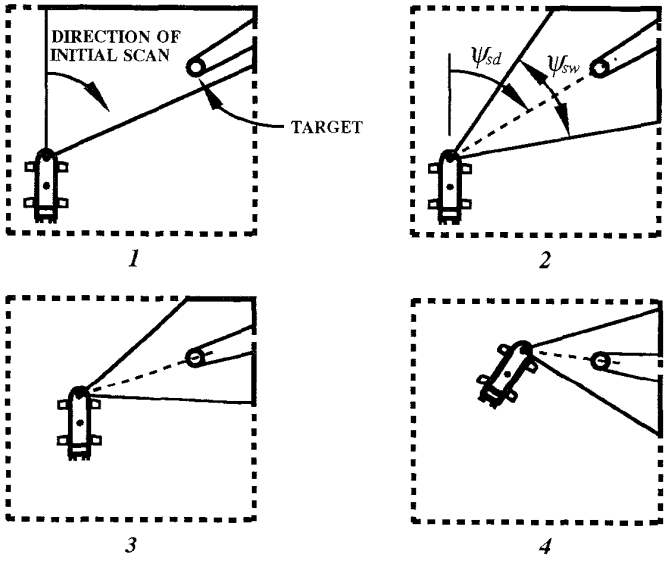

Figure 6. Sonar Scan Patterns for Maneuvers

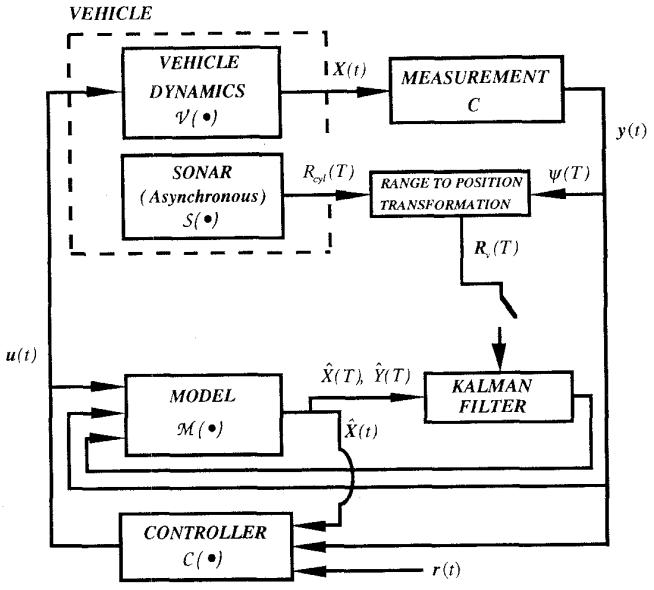

Figure 7. Sonar with Model Control Block Diagram

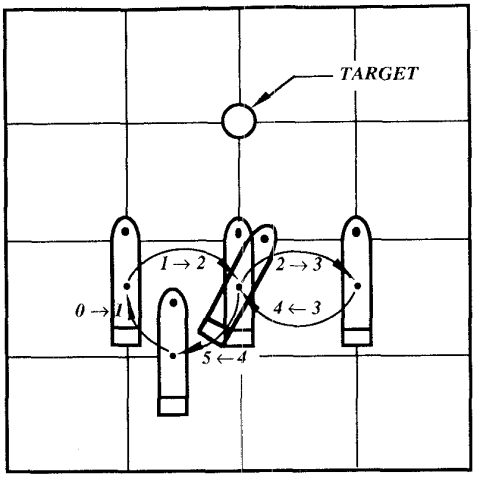

Figure 8. Five Commanded Poses

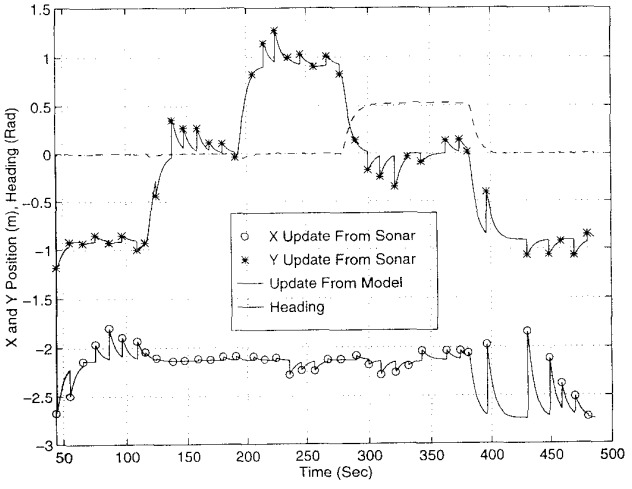

Figure 9. Position Response

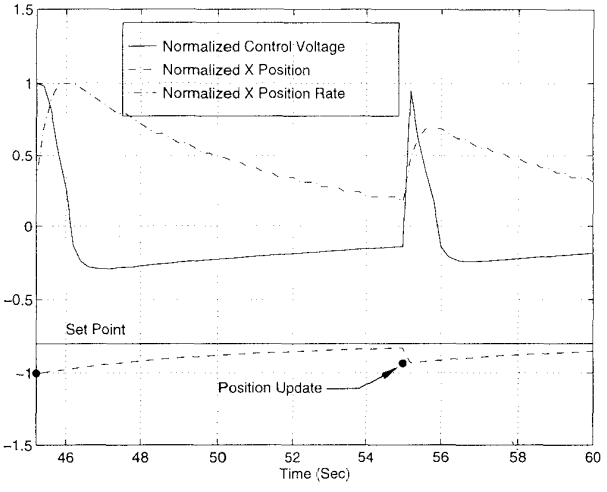

Figure 10. Control Voltage and Longitudinal Response